OPEN

Oncogene (2016) 35, 1811–1821

www.nature.com/onc

ORIGINAL ARTICLE

PML is required for telomere stability in non-neoplastic human cells

M Marchesini[1,2,6,8], R Matocci[1,8], L Tasselli[1,2,7,8], V Cambiaghi[2], A Orleth[2], L Furia[2], C Marinelli[1,2], S Lombardi[2], G Sammarelli[3], F Aversa[3], S Minucci[2,4], M Faretta[2], PG Pelicci[2,5] and F Grignani[1]

Telomeres interact with numerous proteins, including components of the shelterin complex, whose alteration, similarly to proliferation-induced telomere shortening, initiates cellular senescence. In tumors, telomere length is maintained by Telomerase activity or by the Alternative Lengthening of Telomeres mechanism, whose hallmark is the telomeric localization of the promyelocytic leukemia (PML) protein. Whether PML contributes to telomeres maintenance in normal cells is unknown. We show that in normal human fibroblasts the PML protein associates with few telomeres, preferentially when they are damaged. Proliferation-induced telomere attrition or their damage due to alteration of the shelterin complex enhances the telomeric localization of PML, which is increased in human T-lymphocytes derived from patients genetically deficient in telomerase. In normal fibroblasts, PML depletion induces telomere damage, nuclear and chromosomal abnormalities, and senescence. Expression of the leukemia protein PML/RARα in hematopoietic progenitors displaces PML from telomeres and induces telomere shortening in the bone marrow of pre-leukemic mice. Our work provides a novel view of the physiologic function of PML, which participates in telomeres surveillance in normal cells. Our data further imply that a diminished PML function may contribute to cell senescence, genomic instability, and tumorigenesis.

Oncogene (2016) **35,** 1811–1821; doi:10.1038/onc.2015.246; published online 29 June 2015

INTRODUCTION

Chromosomal telomeres surveillance and repair mechanisms continuously operate in proliferating cells to prevent the activation of DNA damage signaling and the development of chromosomal abnormalities. Telomeres structure is protected by a number of proteins constituting the shelterin complex, whose functions include the maintenance of the structure of telomeric DNA loops and the inhibition of the activity of DNA repair proteins, which are found associated with telomeres.[1–3] The protein members of the shelterin complex dynamically interact with telomeric RNAs and with other proteins involved in telomere surveillance, including DNA damage response factors.[4] The shelterin complex exerts a crucial function in the protection of telomeric repeats, since the depletion of its protein members, such as TRF2 and POT1, causes telomere uncapping and damage. As a consequence telomeres associate with a number of proteins, including 53BP1 and gamma-H2AX, constituting the telomere dysfunction-induced focus (TIF), which are considered as markers of telomere damage.[5–7] However, the complex interplay between the shelterin complex and the numerous proteins that engage in transient or stable interactions with telomeric structures is only partially known.

Telomeres surveillance is critical for the regulation of cell life span.[8,9] Indeed, the replication potential of normal cells is limited by a proliferation-dependent telomere attrition, which triggers cell senescence upon excessive shortening of the telomeric DNA repeats.[10,11] Such telomeres attrition leads to progressive modifications of the cell phenotype, which are linked to cellular dysfunctions associated with human aging and age-related disease.[12–14] The maintenance of telomeric DNA repeats length is physiologically necessary to prevent senescence in a few cell types, including stem cells and germ cells. This function is accomplished by the telomerase ribonucleoprotein complex, whose reverse transcriptase component (TERT) elongates telomeric repeats.[15,16] Activation of telomerase occurs also in normal T-lymphocytes when stimulated to proliferate by antigens or lectins, allowing the expansion of an antigen reactive T-cell population.[1] Telomerase becomes abnormally activated in the majority of tumor types, allowing indefinite proliferation of cancer cells.[17] However, 10–15% of tumors do not show telomerase reactivation. In these tumors, the maintenance of telomeres length is accomplished by a telomerase-independent mechanism, referred to as Alternative Lengthening of Telomeres (ALT).[18,19] Hallmarks of ALT are heterogeneity of telomere lengths, circular telomeric DNA, and the association between telomeres and the promyelocytic leukemia (PML) protein.[20] This protein was first discovered as the product of the PML gene, which fuses with the RARα gene in the t(15;17) chromosomal translocation.

[1]General Pathology Section, Department of Experimental Medicine, University of Perugia, Perugia, Italy; [2]Department of Experimental Oncology, European Institute of Oncology, Milan, Italy; [3]Hematology and Bone Marrow Transplantation Unit, Department of Clinical and Experimental Medicine, University of Parma, Parma, Italy; [4]Department of Biosciences, University of Milan, Milan, Italy and [5]Dipartimento di Medicina, Chirurgia e Odontoiatria, Università degli Studi di Milano, Milan, Italy. Correspondence: Professor F Grignani, General Pathology Section, Department of Experimental Medicine, Piazza Lucio Severi, 1, Perugia 06132 Italy or Professor PG Pelicci, Department of Experimental Oncology, European Institute of Oncology, Via Giuseppe Ripamonti, 435, 20141 Milan, Italy.
E-mail: francesco.grignani@unipg.it or piergiuseppe.pelicci@ieo.eu
[6]Present address: Department of Leukemia, MD Anderson Cancer Center, The University of Texas, Huston, TX, USA.
[7]Present address: Division of Endocrinology, Gerontology, and Metabolism, Department of Medicine, Stanford University School of Medicine, Stanford, CA, USA and Geriatric Research, Education, and Clinical Center, VA Palo Alto Health Care System, Palo Alto, CA, USA.
[8]These authors contributed equally to this work.
Received 22 November 2014; revised 13 April 2015; accepted 10 May 2015; published online 29 June 2015

This chromosomal abnormality causes the human acute promyelocytic leukemia (APL), where a fusion PML/RARα protein is expressed.[21–24] In normal cells, the PML protein aggregates nuclear structures called PML nuclear bodies (PML-NBs), where it interacts with multiple protein partners to accomplish a wide variety of functions, including regulation of transcription and p53 activation.[25,26] PML also participates in DNA damage response and is overall regarded as a tumor suppressor.[27–30] The interaction between the PML protein and telomeres is clearly recognized in ALT cells, where the PML protein is present within telomeric bodies named ALT-associated PML nuclear bodies.[20] However, the specific role played by the PML protein in this context is still under investigation. Another fundamental question is whether PML-NBs exert a telomeric function in normal cells. Evidence for the presence of the PML proteins at the telomeres of non-neoplastic cells have been reported in human endothelial cells and mouse embryonic stem cells, where the PML protein appears to be relevant for telomeres stability.[31,32] However, it is not clear whether this localization is functionally significant nor if it has a role upon proliferative telomeric attrition or damage. Another open question is whether an altered function of the telomeric PML could contribute to the pathogenesis of leukemia. The PML/RARα protein[33] acts as a transcriptional repressor of RARα and non-RARα target genes and disrupts the PML-NBs exerting a dominant negative activity on their function.[25,34] Whether the leukemogenic function of the PML/RARα protein involves an alteration of the function of PML at telomeres is still unknown.

In this paper, we characterize the telomeric localization and function of the PML protein in non-neoplastic cells. We show that PML/telomere associations increase upon proliferative telomere attrition and telomeric damage. PML depletion causes telomeric damage, genomic instability and cell senescence, indicating a critical role for PML in telomeres surveillance. Moreover, the PML/RARα fusion protein displaces PML from telomeres and induces telomeres shortening in human hematopoietic precursor cells, identifying a novel contribution to APL leukemogenesis.

RESULTS

The PML protein localizes at telomeres in normal cells

We investigate the localization of PML at telomere in cell types with different telomere maintaining mechanisms. To this end, we performed telomeric fluorescence *in situ* hybridization (FISH) analysis combined with immunofluorescence for PML (immuno-FISH) in interphase ALT tumor cell lines (U2-OS, SK-LU-1 and SA-OS-2), normal human fibroblasts (WI38, MRC-5), mouse embryonic fibroblasts and telomerase-positive cancer cell lines (HeLa and A549 and U937) (Figure 1a and Supplementary Figures 1a–c). 3D reconstructions shown in Supplementary Figure 2 and Supplementary video 1 illustrate the standards for colocalization scoring. As expected, in ALT cell lines we observed that 30–80% of the PML-NBs colocalized with telomeres (Figure 1b and Supplementary Figure 1). Normal human and mouse fibroblast cells and telomerase-positive cancer cells also showed colocalization between PML-NBs and telomeres, although at much lower frequency than ALT cell lines (Figure 1b and Supplementary Figure 1d). The percentage of PML-NBs at telomere in non-ALT cells was small but consistent, ranging from 4 to 14% of total PML-NBs number in normal fibroblasts and 22–35% in telomerase-positive cells, independently from the number of PML-NBs per cell. In the different cell lines, the number of PML-telomere colocalization per cell ranged from 0.36 to 5.86 (Supplementary Figure 1d). Thus, a fraction of the PML protein colocalizes with telomeres in telomerase-positive cancer cells and in non-neoplastic cells, suggesting an extended and physiologic function for PML at telomere.

PML association with telomeres increases upon telomeres attrition

We thereafter focused on non-neoplastic cells and asked whether the PML protein may contribute to telomere surveillance during specific phases of the cell cycle, since telomere replication is a critical process, requiring accurate care.[35] Considering the low frequency of the telomeric localization of PML, we took advantage of an automated fluorescence image analysis,[36,37] allowing the study of a large number of cells and their cell-cycle phase (Figures 2c–f). MRC5 normal human fibroblasts were stained with anti-PML, -TRF2 and -53BP1 antibodies, in association with DAPI incorporation to detect DNA amount and Ethinyl-Deoxyuridine (EdU) staining, which allows replication measurement (Figures 2a and d). This procedure allowed (i) the detection of telomeres, as identified by TRF2 signals, (ii) the detection of damaged telomeres as damage induced foci (TIFs), identified by measuring 53BP1-TRF2 overlap in the proximity ligation assay[36,37] (PLA, Figure 2b); (iii) the identification of the cell-cycle phase and (iv) the analysis of the PML/telomeres and damaged telomeres colocalization. We detected an average of 0.65 PML-telomere colocalizations per cell (Figure 2c). The distribution of the number of PML-NBs and the PML/TIF colocalizations, depending on the DNA content of the cells (Figures 2d–f), did not show statistically significant differences, indicating that the telomeric function of PML is not specific for a cell-cycle phase. When we compared proliferating and late passage (see Materials and methods) near senescent (NS) cells,[8–10]

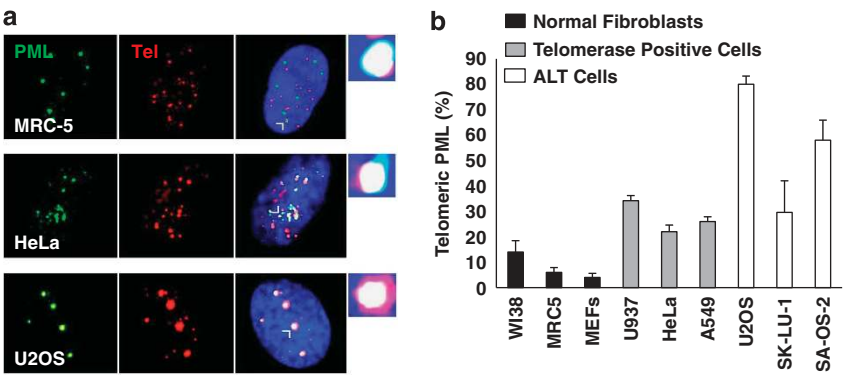

Figure 1. PML associates with telomeres in telomerase-positive and non-neoplastic cells. (**a**) Confocal images of a representative immuno-FISH experiment performed with anti-PML antibodies (green, Alexa488) and a telomeric PNA probe (red, Cy3) in normal human fibroblast (MRC5) a telomerase-positive cell line (HeLa) and an ALT cell line (U2OS). PML/Tel colocalizations were identified as overlapping signals in cell nuclei evidenced by DAPI staining. An enlargement of the colocalizing signals pointed by the arrows is shown on the right. (**b**) Quantitative analysis of immune-FISH experiments for PML-telomere colocalization in WI38, MRC-5 (normal human fibroblasts), mouse embryonic fibroblasts (MEFs), U937, HeLa, A549 (telomerase-positive cancer cells) and U2OS, SK-LU1, SA-OS-2 (ALT-positive cancer cells). Fifty cells per type were scored in each of three experiments. The percentage of PML-NBs co-localizing with telomeres is shown as average ± s.d.

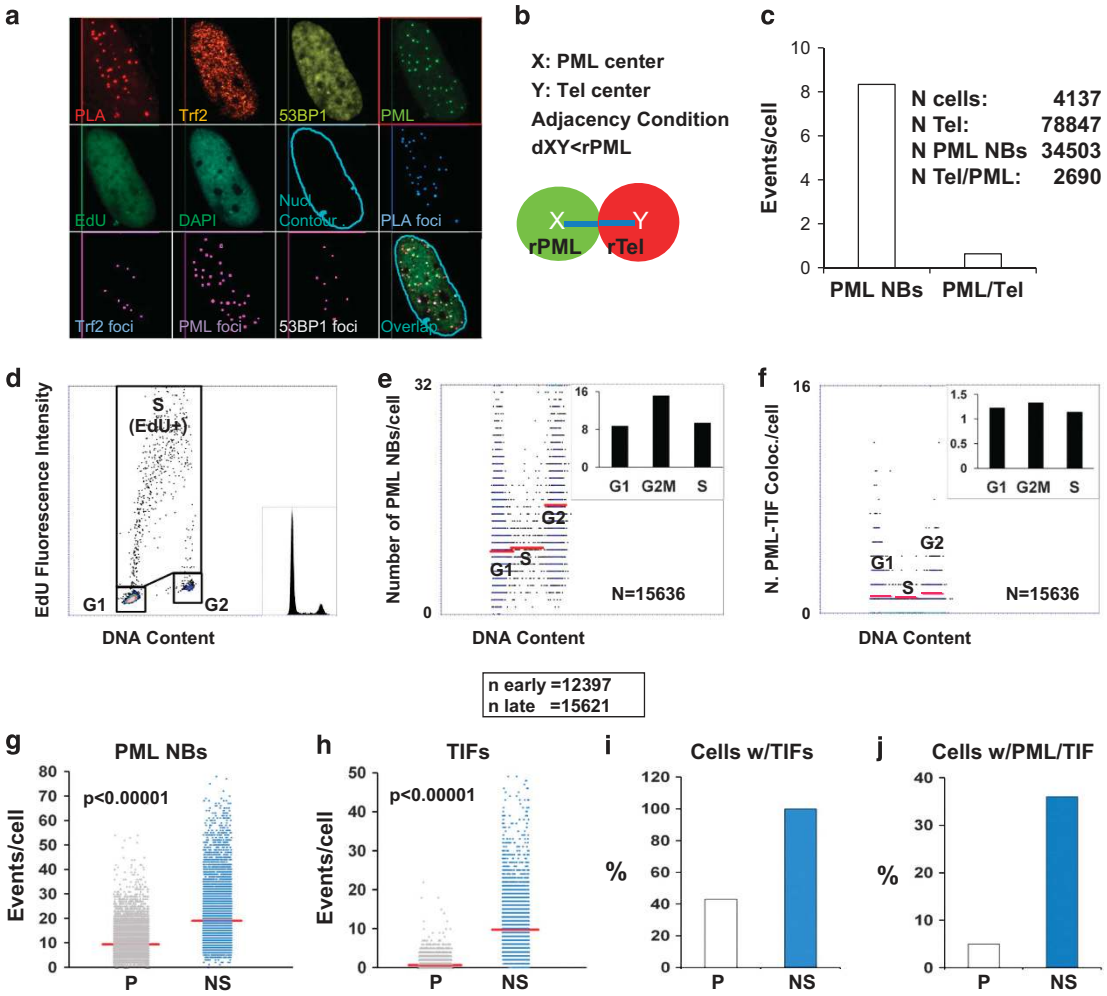

Figure 2. Automated Image Cytometry Analysis of PML-telomere association. (**a**) Images from automated Image Cytometry Analysis on MRC5 cells. The cells were stained with fluorescent antibodies conjugated with different dyes against 53BP1 (Pacific Orange), TRF2 (Alexa 647), PML (Alexa 488); DNA was stained with (DAPI) and EdU (Pacific Blue). Damaged telomeres were analyzed by PLA to detect 53BP1 and Trf2 proximity (see text and Materials and methods). PLA foci, Trf2 foci, PML foci and 53BP1 foci indicate the electronic signals automatically identified by the computer within the indicated nuclear contour. The overlap of all the fluorescences is shown in the last panel. (**b**) Parameters of computational analysis for the Image Cytometry Analysis software; dXY: distance of the X and Y centers; rPML, rTel: radius of the signal; (**c**) Average number of PML-NBs and the average number of their colocalization with telomeres per cell in a representative experiment. The total number of cells, telomeres, PML-NBs and colocalizations is indicated. (**d**) EdU-DNA content dot plot showing the procedure to identify cell-cycle phases, as explained in Materials and methods. The inset shows the DNA content distribution of the analyzed population of cells ($n = 15\,636$). (**e**) Bivariate dot plot reporting on the X axis the DNA content and on the Y axis the number of colocalization PML signals per cell of PML and Trf2 bodies. The insert shows the average number of PML signals in each cell-cycle phase as identified by the analysis. (**f**) Bivariate dot plot reporting on the X axis the DNA content and on the Y axis the number of PML bodies per cell. The insert shows the average number of events in each cell-cycle phase as identified by the analysis; the number of analyzed MRC5 exponentially growing cells is indicated. (**g**, **h**) Average number of PML-NBs or TIFs, as scored by analysis of the indicated number of proliferating (P) or late passage NS cells, as indicated and defined in the Materials and methods. Statistical significance has been calculated by a two-tailed Student's *t*-test. (**i**, **j**) Representative experiments showing the percentage of cells with at least one TIF or one PML/TIF colocalization. TIF scored by PLA between Trf2 and 53BP1 protein.

the number of TIFs and PML-NBs increased in the latter (Figures 2g and h),[26] where most of the cells displayed at least one TIF (Figure 2i). In these experiments, a fraction of the telomeric PML colocalized with dysfunctional telomeres (TIFs), as 5% of proliferating cells displayed PML/TIFs colocalization. Notably, this percentage increased to 36% of the NS cells (Figure 2j).

To further investigate the link between senescence-associated telomere attrition with and recruitment of the PML protein at telomere, we analyzed proliferating and NS WI38 fibroblasts by immuno-FISH, using anti-PML and anti-γH2AX antibodies staining together with a PNA telomeric probe (Figure 3a). The number of TIFs per cell, as identified by overlapping γH2AX and telomeric signals, increased in NS WI38 cells (Figure 3b). The number of PML-NBs and the number of their colocalization with telomeres and TIFs increased significantly (Figure 3b and Supplementary Figure 3a and b). Moreover, the percentage of the total NBs associated with telomeres (PML/Tel%) and with TIFs (PML/TIFs%) was almost double in NS than in proliferating cells (Figure 3b). Overall, these results indicate that physiologic, proliferation-induced attrition triggers PML colocalization with telomeres.

We next asked whether the localization of PML at telomeres could be specifically relevant in the context of telomere attrition due to premature senescence. To this end, we studied IL-2 stimulated peripheral blood T-lymphocytes from a patient

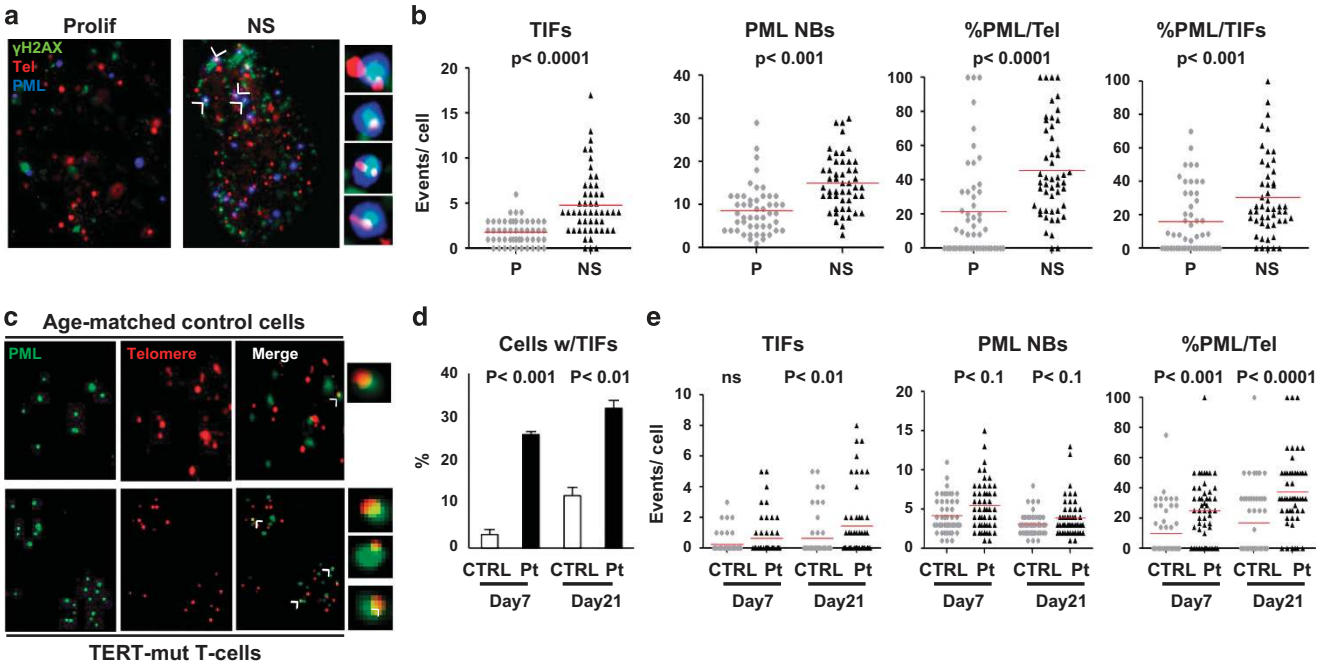

Figure 3. PML association with telomeres increases upon telomeres attrition. (**a**) Representative immune-FISH experiments on WI38 normal proliferating (P) or late passage NS human fibroblasts. Merged images of the fluorescence signals produced by a telomeric probe (red, Cy3), anti-PML (Cy5) or anti-γH2AX antibodies (green, Alexa488). Enlargements of triple overlapping signals are shown. (**b**) Quantitative analysis of experiments as in (**a**). Each dot represents one of fifty cells analyzed in one experiment representative of three. The average values (red lines) indicate the number of TIFs ± s.d. (1.78 ± 0.19 in proliferating and 4.86 ± 0.5 in NS cells) or PML-NBSs per cell (8.72 ± 0.79 in proliferating and 15.06 ± 0.9 in NS cells), the percentage of PML-NBSs colocalizing with telomeres (PML/Tel%: 21.62 ± 4.08 in proliferating and 45.83 ± 3.9 in NS cells) and the percentage of PML-NBSs colocalizing with TIFs (PML/TIFs% 16.03 ± 2.75 in proliferating and 30.56 ± 3.39 in NS cells), as detected by triple γH2AX/telomeres/PML signals colocalization. (**c**) Representative immuno-FISH experiment performed on normal age-matched control (CTRL) and TERT-mutated IL-2 stimulated peripheral blood T cells, using a telomeric PNA probe (red, Cy3) and anti-PML antibodies (green, Alexa488) and merged images. Enlargements of PML/Telomere colocalizations are shown on the right. (**d**) Quantitative analysis of experiments as in (**c**), on IL-2 stimulated normal (CTRL) or TERT-deficient T-cells (Pt) at culture days 7 (d7) and 21 (d21). Percentage of cells with TIFs (average ± s.d. from three independent experiments: day 7 CTRL 3.1 ± 0.19, Pt 26.1 ± 0.45; day 21 CTRL 12.0 ± 0.53, Pt 32.1 ± 0.75). (**e**) Quantitative analysis of immune-FISH experiments performed as in (**a**). The average values (red lines) indicate the number of TIFs or PML-NBSs per cell and the percentage of PML-NBs colocalizing with telomeres (% PML/Tel). (TIFs: day 7, CTRL 0.26 ± 0.09, Pt 0.66 ± 0.18; day 21, CTRL 0.64 ± 0.19, Pt 1.46 ± 0.33 PML-NBs: day 7, CTRL 4.22 ± 0.32, Pt 5.48 ± 0.44; day 21, CTRL 3.1 ± 0.19, Pt 3.92 ± 0.34; %PML/Tel day 7, CTRL 10.2.7 ± 2.27, Pt 25.2 ± 2.87; day 21, CTRL 16.9 ± 3.16, Pt 37.6 ± 3.42). The *P*-values are based on a two-tailed Student's *t*-test.

carrying a germline mutation of the TERT gene, resulting in TERT aploinsufficiency (Figures 3c and e). In immuno-FISH experiments, the number of PML-NBs, identified in patient's cells was similar to that of age-matched control T-lymphocytes and remained relatively stable during prolonged *in vitro* culture (Figure 3e). However, the number of TIFs was higher in TERT mutated T-lymphocytes than in controls and increased with *in vitro* culture (Figure 3d), indicating augmented telomere attrition. Significantly, the percentage of PML-NBs colocalizing with telomeres (PML/Tel) was higher in TERT-deficient cells and further increased to more than double than control cells upon cell proliferation in culture (Figure 3d), suggesting a progressive recruitment of PML to proliferation-induced dysfunctional telomeres.

Specific telomeric damage increases PML localization at telomeres

The above data suggested that PML may participate in damaged telomeres surveillance. Thus, we measured PML/telomere colocalization after the induction of telomere-specific damage. The G-quadruplex ligand RHPS4 delocalizes POT1 from telomeres and induces TIFs formation.[38,39] We treated early passage WI38 normal human fibroblasts with RHPS4 for 24 h and performed immuno-FISH staining (Figure 4a). In exponentially growing cells, the treatment induced a significant increase in TIFs number (Figure 4b). PML-NBs increased in number (Figure 4b) and were recruited to telomeres, as shown by a threefold increase in the number of PML/telomere colocalizations (Supplementary Figure 3c) and by a 3.5-fold raise in the percentage of PML-NBs colocalizing with telomeres (Figure 4b). Moreover, the number of colocalizations between PML-NBs and TIFs markedly increased (Supplementary Figure 3d) and the percentage of total PML-NBs colocalizing with TIFs increased by tenfold, as compared with control cells (Figure 4b).

To investigate the interaction of the PML protein with uncapped telomeres, we depleted the TRF2 protein[40] in early passage WI38 and MRC5 normal human fibroblasts by lentivirus-mediated short hairpin RNA (shRNA) interference (TRF2 KD), using as a control a vector carrying a shRNA directed against a luciferase sequence (CTRL). After cell selection, TRF2 depletion was verified by western blotting and immunofluorescence assays (Supplementary Figures 4a and b). In agreement with previous reports,[5] WI38 and MRC5 human fibroblasts infected with a TRF2KD vector, but not with the control vector, displayed a significant increase in TIFs and PML-NBs (Figures 4c and d and Supplementary Figures 4c and d). The number of PML colocalizations with telomeres and specifically with TIFs increased markedly in both TRF2-depleted WI38 and MRC5 cells, as compared with controls (Supplementary Figure 4e and f). This increase is not a consequence of the increased number of PML-NBs in TRF2-depleted cells, since, the percentage of the total PML-NBs colocalizing with telomeres raised markedly and the percentage of PML-NBs specifically associated with TIFs increased more than 25- and 35-fold in WI38

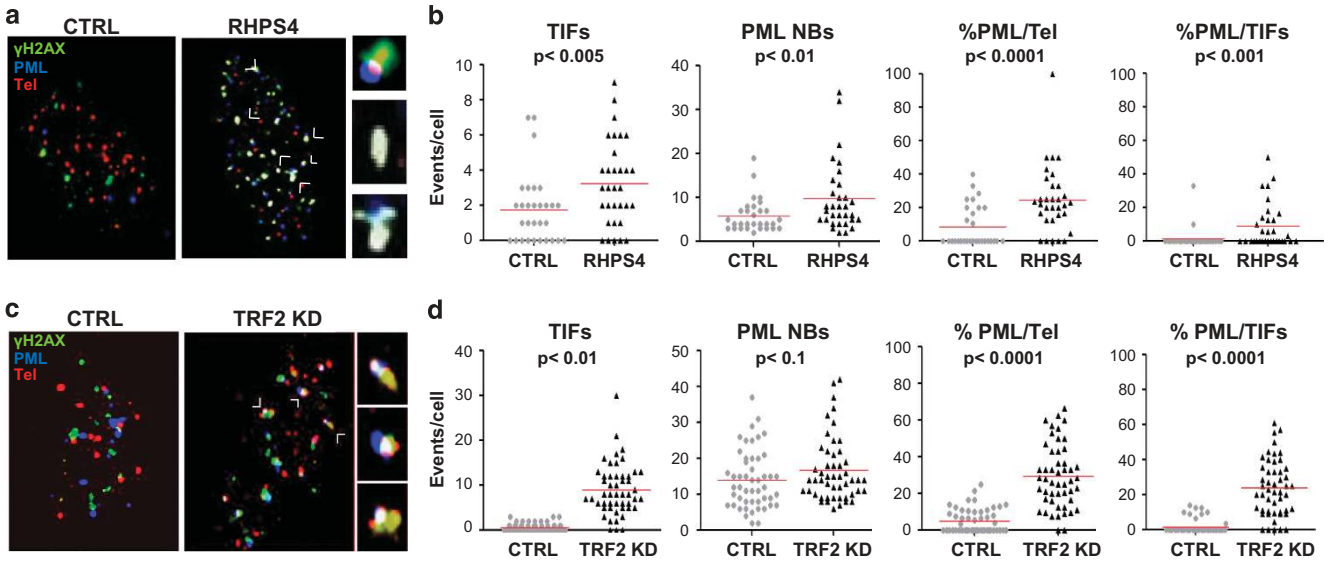

Figure 4. PML associates with damaged telomeres. (**a**) Representative immuno-FISH experiments on WI38 normal human fibroblasts, before and after specific telomeric damage induced by RHPS4 treatment. Merged images generated by a telomeric PNA probe (red, Cy3) and anti-γH2AX (green, Alexa488) or anti-PML (blue, Cy5) antibodies. Enlargements of triple overlapping signals are shown on the right. (**b**) Quantitative analysis of the immune-FISH experiments shown in (**a**). Each dot represents one of fifty cells analyzed in each of three experiments and counted before (CTRL) and after RPHS4 treatment. The average values (red lines) show the number of TIFs per cell (1.77 ± 0.36 before and 3.25 ± 0.43 after treatment) or PML-NBs per cell (5.9 ± 0.7 before and 9.78 ± 1.39 after treatment), the percentage of PML-NBs colocalizing with telomeres (%PML/Tel: 8.38 ± 2.25 before and 24.77 ± 3.55 after treatment) and the percentage of PML-NBs colocalizing with TIFs (%PML/TIFs: 1.44 ± 1.15 before and 8.88 ± 2.37 after treatment) as detected by triple γH2AX/telomeres/PML signals colocalization. (**c**) Representative immuno-FISH experiment, performed as in (**a**), on WI38 cells before (CTRL) after (TRF2 KD) TRF2 RNA interference. Three enlargements of triple overlapping signals are shown. (**d**) Quantitative analysis, as in (**b**), of immune-FISH experiments performed on WI38 cells before (CTRL) after (TRF2 KD) TRF2 RNA interference. TIFs 0.72 ± 0.13 in control and 9.04 ± 0.81 in TRF2 KD cells; PML-NBs 14.0 ± 1.14 in control and 17.0 ± 1.25 in TRF2 KD cells; % PML/Tel 5.28 ± 0.94 in control and 29.5 ± 2.44 in TRF2 KD cells; % PML/TIFs 1.75 ± 0.57 in control and 23.99 ± 2.26 in TRF2 KD cells. The *P*-values indicated in (**b**) and (**d**) are based on a two-tailed Student's *t*-test.

and MRC5 cells, respectively (Figure 4d and Supplementary Figure 4d). Overall, these data show that telomere damage induced by loss of components of the shelterin complex causes PML association with altered telomeres.

PML depletion leads to telomere dysfunction and senescence in non-neoplastic cells

To unveil the role of the PML protein at telomere in normal cells, we depleted its expression in early passage WI38 and MRC5 cells. To this end, we infected and selected the cells using two PML shRNA lentiviral vectors (PML KD1 and PML KD2) targeting exon 3 sequences common to all the PML isoforms (Figure 5a). Strikingly, PML knockdown caused a dose-dependent decrease in cell proliferation (Figure 5a), morphological changes consistent with a senescent phenotype and an increased expression of the senescence-related β-galactosidase enzyme (Figures 5b and c). Moreover, a senescence molecular pathway was activated, as shown by an increased expression of the p53, $p16^{INK4a}$ and $p21^{WAF1}$ proteins in PML-depleted cells with respect to control cells (Figure 5d). Significantly, PML depletion did not induce senescence, proliferation arrest or reduced clonogenicity in the telomerase-positive HeLa cell line (Supplementary Figure 5). To investigate whether this phenotype was linked to the role of PML at telomeres, we measured the generation of TIFs upon PML depletion (Figure 5e). The data showed a significant increase in TIFs formation in both WI38 and MRC5 PML-KD cells with respect to control cells, indicating that PML depletion induces telomeric damage (Figure 5f). Immuno-FISH experiments employing a PNA telomeric probe, anti-γH2AX and anti-p53 antibodies, showed that the number of p53-positive cells was markedly increased in PML-KD MRC5 cells (Figures 5g and h). More than 90% of PML-KD p53-positive cells were TIF positive (Figure 5i), indicating that telomere dysfunction was most likely the trigger for p53 activation. Taken together, these data show that PML contributes to telomere integrity in normal cells and that its depletion causes telomeric damage and the activation of premature senescence.

PML depletion is associated with chromosomal abnormalities and genomic instability

The above data uncover the role of PML in maintaining telomere integrity of normal human fibroblasts. To further investigate the relevance for chromosomal stability of PML activity at telomeres, we analyzed nuclear abnormalities in MRC5 cells after siRNA-mediated PML depletion. More than 20% of cells displayed binucleation (Figures 6a and b). To emphasize defects in nuclear division, we treated the cells with blebbistatin, a cytokinesis inhibitor. DAPI stained nuclei showed several abnormalities, including nucleoplasmic bridges (NPBs), micronuclei (MNs) and nuclear buds (Buds) (Figures 6c and d), which are considered hallmarks of genomic instability due to telomeric dysfunction.[41] These abnormalities were scored in $>50\%$ of PML-depleted cells (Figure 6d). To link these observations with telomere dysfunction, we analyzed chromosome spreads of control and PML-KD MRC5 cells and performed telomeric FISH to investigate the status of chromosome ends. Chromosomes of PML-KD MRC5 cells showed a number of aberrations, including end-to-end fusion, circle chromosomes and fragile telomeres (Figures 6e and f). These abnormalities most likely derive from the telomeric dysfunction associated with PML depletion. In addition, the metaphases showed chromosomal breaks and fragments (Figure 6f), which seemingly indicate the development of genomic instability. Overall, PML depletion in normal human fibroblast cells is associated with telomere dysfunction and chromosomal instability, leading to senescence induction.

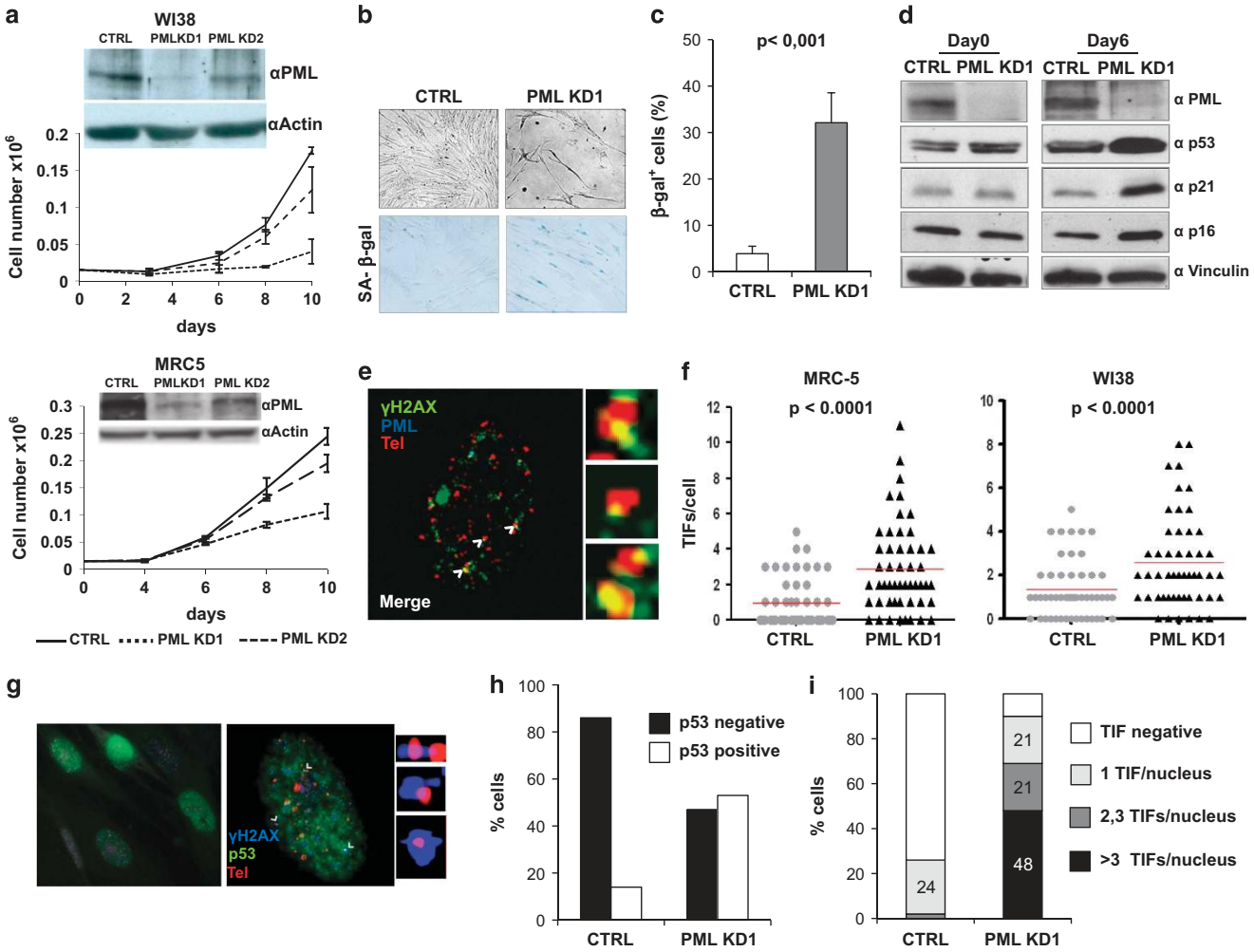

Figure 5. PML depletion leads to telomere damage and senescence in human fibroblasts. (**a**) Growth of WI38 and MRC5 cells infected with PML shRNAs KD1 or KD2 or control luciferase shRNA (CTRL). Cells were counted at the indicated times after 6 days of puromycin selection. The error bars indicate the s.d. of the counts obtained in three experiments. Above the curves is a representative western blotting with the indicated antibodies, from cells lysed at day 3 after selection. (**b**) Microphotographs of control (CTRL) or PML knockdown (PML KD1) WI38 cells at 6 days post selection, unstained or stained for SA-β-galactosidase. (**c**) Quantitative analysis of SA-β-gal-staining on the cells shown in (**b**). (**d**) Western blotting with the indicated antibodies on the indicated WI38 cells lysed after 6 days of PML RNAi. (**e**) Representative immuno-FISH experiment on MRC-5 cells infected with PML-KD1: merged image of the signals obtained with a telomeric probe (red, Cy3) and anti-γH2AX (green, Alexa488) and anti-PML (blue, Cy5) antibodies. Enlarged PML/TIF colocalization images are shown on the right. (**f**) Quantitative analysis of immuno-FISH experiments performed as in (**e**), showing the number of TIFs per cell in MRC5 and WI38 cells, before (CTRL) and after PML knockdown (PML KD). Each dot represents one of the fifty cells analyzed in each of three experiments. The average value (red line) shows the number of TIFs per cell (0.96 ± 0.19 in Control and 2.9 ± 0.36 PML KD MRC5 cells and 1.34 ± 0.19 in control or 2.6 ± 0.3 in PML KD WI38 cells, respectively). The *P*-value was obtained by a two-tailed Student's *t*-test. (**g**) Representative immuno-FISH experiment performed on PML-depleted MRC-5 cells using a telomeric probe (red, Cy3) and anti-p53 (green, Alexa488) and anti-γH2AX (blue, Cy5) antibodies; notably, very few apoptotic nuclei were detected in PML-depleted cells without a significant increase as compared with control cells. Enlargements of a single p53-positive cell and TIFs are shown on the right. (**h**) Quantitative evaluation of p53-positive MRC5 cells after the infection with a control vector (CTRL) or the PML-KD1 vector. (**i**) Quantitative analysis of immuno-FISH experiments indicating the percentage of p53-positive cells showing the indicated number of TIFs per cell. The experiments shown in (**h**) and (**i**) are representative of three.

The telomeric function of PML is hampered by the APL PML/RARα protein

Leukemia cells in APL have short telomeres.[42] Since the APL fusion protein PML/RARα disrupts PML-NBs,[25] we investigated whether an impairment of the telomeric function of PML could contribute to the pathological activity of PML/RARα. To this end, we infected normal human CD34+ hematopoietic progenitor cells (HPCs) in liquid culture with a retrovirus vector expressing PML/RARα or a control vector and analyzed the PML/telomere colocalization (Figure 7a), using the criteria illustrated in Supplementary Figure 1. In these conditions, normal HPCs showed at least one PML/Telomere colocalization event in about 50% of the cells. However, in PML/RARα expressing HPCs colocalization was only found in 15% of the cells (Figure 7b). Moreover, 50% of the control cells had >10% of the PML signals colocalizing with telomeres whereas this was observed in only 3% of the PML/RARα cells (Figure 7c). Overall, these data indicate that PML/RARα expression impairs PML association with telomeres. To investigate whether this fact could relate with the telomere shortening of APL blasts, we analyzed bone marrow cells derived from the pre-leukemic stage of mice transplanted with PML/RARα expressing Lin− hematopoietic progenitors.[43] We found that telomeres displayed a 20% average reduction in length (Figure 6d), indicating that, before the development of leukemia, the expression of PML/RARα and displacement of PML from telomeres correlate with an overall reduction of telomeres length.

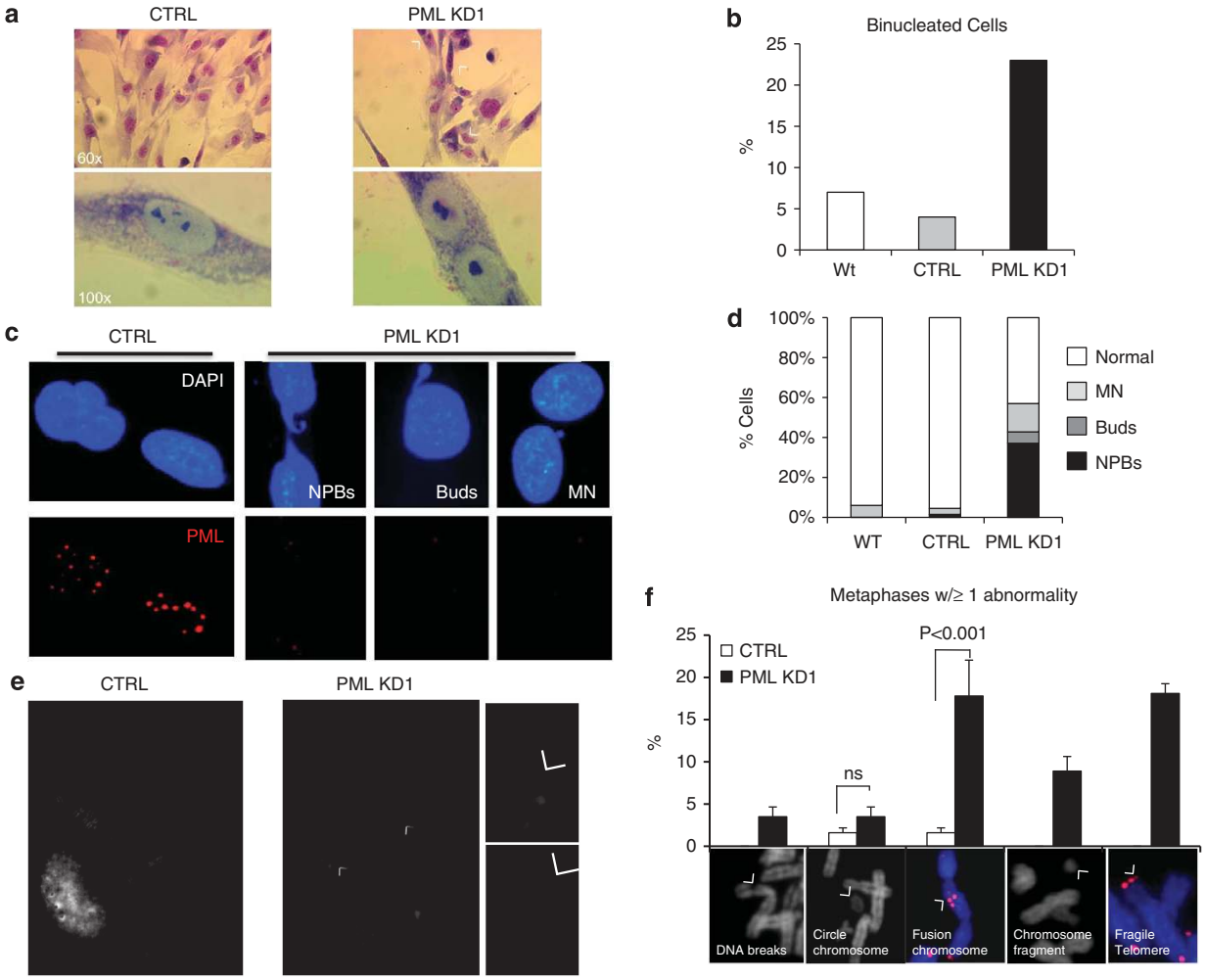

Figure 6. PML depletion causes nuclear and chromosomal abnormalities in human fibroblasts. (**a**) Microphotographs at the indicated magnification of MGG-stained slides of MRC5 cells, transfected with a control non-specific siRNA (CTRL) or PML-KD1 siRNA (PML-KD) for PML RNA interference. (**b**) Percentage of binucleated cells counted in wild type (Wt), control (CTRL) and PML KD MRC5 cells relative to total asynchronous events evaluated by DAPI staining. A representative experiment of three is shown. One hundred cells were analyzed in each experiment. (**c**) DAPI nuclear staining (DAPI) and immunofluorescence with anti-PML antibodies (PML) on control (CTRL) or PML KD MRC5 cells, treated with blebbistatin to block cytokinesis. Representative images of NPBs, MNs and nuclear buds (Bs) in PML-depleted cells. (**d**) Quantitative analysis of overall nuclear abnormalities in PML-depleted cells. NPBs, MNs and Bs were counted and percentages calculated with respect to total cells. A representative experiment of three is shown. One hundred binucleated cells were analyzed in each experiment. (**e**) Metaphase spreads of control (CTRL) and PML-depleted (PML KD) MRC-5 cells, as above. Examples of chromosomal aberrations are enlarged on the right. (**f**) Chromosome aberration analysis in control (CTRL) and PML-depleted (PML KD) cells, as above. Bars represent metaphases with at least one aberration events as a percentage of all the scored metaphases. The error bars indicate the s.d. of the counts obtained in three experiments where 50 metaphases were analyzed. The *P*-value was obtained by a two-tailed Student's *t*-test.

DISCUSSION

This study shows that the PML protein may participate in telomeric surveillance in non-neoplastic cells. The low levels of telomeric damage generated by *in vitro* culture of early passage normal human fibroblasts in exponential proliferation are sufficient to induce the telomeric localization of PML. Telomerase-positive tumor cell lines also displayed telomeric PML signals, overall extending the telomeric localization of PML beyond the neoplastic ALT cells displaying ALT-associated PML bodies.[20] These data are in agreement with reported observations obtained in human umbilical vein endothelial cells, telomerase-positive cancer cell lines[44] and mouse embryonic stem cells.[32] The telomeric localization of the PML protein in normal cells is a low frequency phenomenon. We therefore used an automated confocal microscopy method,[36,37] which allowed us to precisely quantify PML/telomere colocalization in a large number of cells, while relating the findings to the cell-cycle phase. Telomere replication is a critical step in the cell cycle. Capping proteins must dissociate from telomeres making them accessible for DNA replication factors and regulatory proteins, whereas DNA damage protein is transiently recruited to telomeres during G2/M phase.[45] However, we found that the association of PML-TIFs is not cell-cycle phase dependent suggesting that PML exerts its function independently from telomeric DNA replication. In normal human fibroblasts, PML interacts with telomere at a much lower frequency than in ALT tumor cells. Most likely, this is due to the more prominent telomere damage and instability in tumor cells activating the ALT system. The abundance of telomeric PML protein in ALT cells may suggests that PML is recruited to damaged telomeres. Whether this hypothesis could hold true in normal cells is not clearly established, although an activation of the ALT pathway has been reported upon radiation induced general DNA damage.[46] We addressed this issue in diverse model systems. First, we quantitatively analyzed telomeric PML in NS

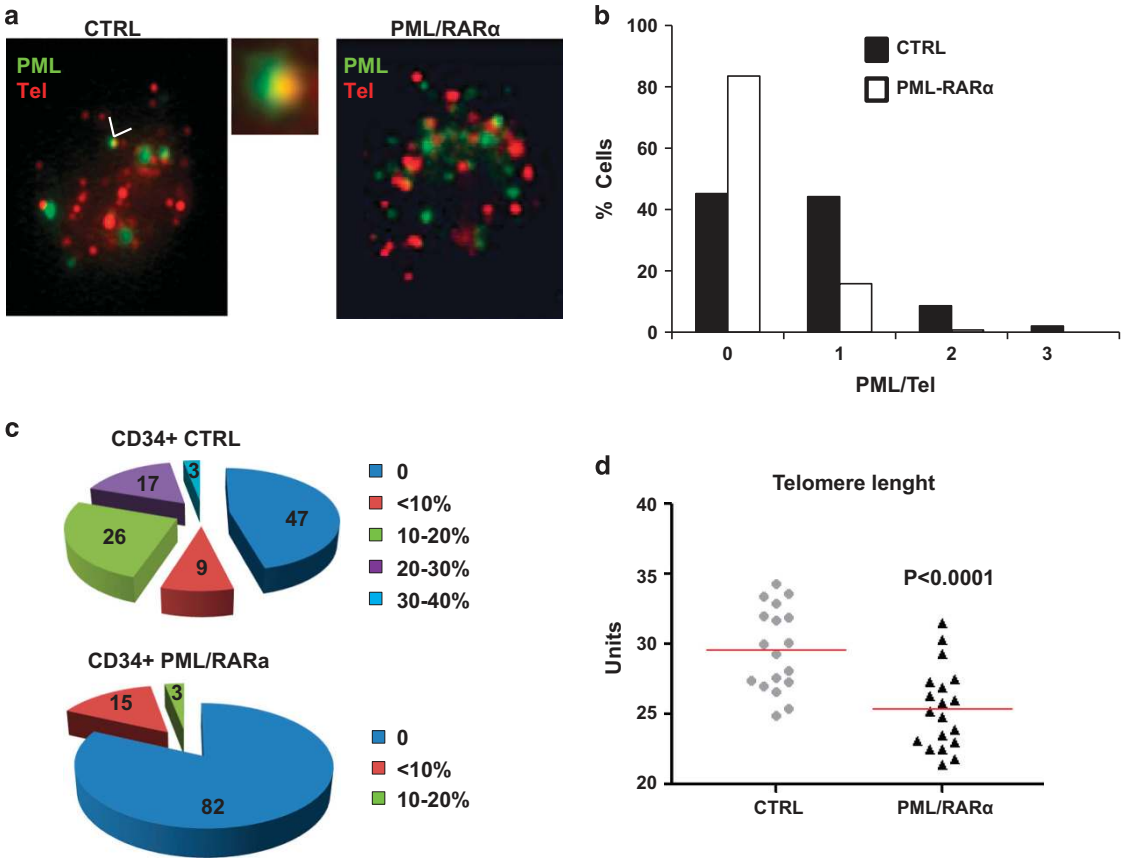

Figure 7. The expression of the APL fusion protein PML/RARα impairs the telomeric function of PML. (**a**) Representative image from immuno-FISH experiments with a telomere probe (red, Cy3) and an anti-PML antibody (Alexa488), performed in human CD34+ HPCs infected with a control vector (CTRL) or a PML/RARα expressing vector. An enlargement of a PML/Telomere colocalization detected in CTRL cells is shown. (**b**) Percentage of cells with the indicated number of PML/telomere colocalization in control or PML/RARα expressing human CD34+ HPCs in a representative experiment of three. 100 cells were analyzed. (**c**) Percentage of CD34+ human HPCs with the indicated percentage of PML signals colocalizing with telomeres in a representative experiment. In control cells (CTRL) PML-NB were counted. In PML/RARα expressing cells microspeckles were counted. 100 cells were analyzed. One representative experiment of three is shown. (**d**) Telomere length in murine bone marrow cells obtained between 2 and 4 months after transplant with syngeneic Lin− bone marrow cells, infected *in vitro* with a control retroviral vector (CTRL) or a PML/RARα expressing vector. Telomeres length is expressed in arbitrary fluorescence units relative to a standard curve. Each dot represents a mouse. A red line indicates the average value: CTRL 29.7 ± 4.6 s.d. PML/RARα 25.8 ± 4.9 s.d. The indicated *P*-value is based on a two-tailed Student's *t*-test.

fibroblast cells. We found that PML associates with telomeres undergoing attrition upon cell passage *in vitro*, specifically colocalizing with damaged telomeres. Thus, PML interacts with telomeres when they are physiologically shortened during cell proliferation. An accelerated telomere shortening is seen in rare syndromes caused by mutations in components of the telomerase complex.[47] Indeed, we found that T-lymphocytes derived from a patient carrying a germline mutation of the TERT gene diffusely displayed a higher number of TIFs, with respect to age matched controls. TIFs increased further upon *in vitro* culture and the percentage of PML-NBs co-localizing with telomeres was much higher than in control cells, confirming an association of PML with shortened telomeres. Thus, it can be speculated that PML may participate in telomere surveillance and stability during cellular senescence and, possibly, human aging.

We also asked whether PML might participate in the surveillance on telomere damage induced by alterations in the shelterin complex. We specifically induced telomere damage in normal fibroblasts by treating the cells with the drug RHPS4, which delocalizes POT1 from telomeres[39] or by depleting the cells of TRF2, an essential component of the shelterin complex.[40] In both cases, the association of PML with damaged telomeres increased markedly. These data support the view that, in non-neoplastic cells, PML comes into play when telomeres are damaged by diverse causes, thus participating in physiologic telomere homeostasis. The effects of PML depletion observed in normal cells support this novel prospect on PML function. An inadequate amount of PML induces the activation of a senescence program, including an increased expression of p53, p21 and p16, and undergo proliferation arrest. In these conditions, we did not observe significant changes in cell death, suggesting that senescence is the major mechanism activated by PML depletion. Moreover, PML-depleted cells develop nuclear and chromosomal abnormalities indicating that a defective PML function is associated with chromosomal instability. A decreased activity of PML on genomic DNA damage foci[27,48] could contribute to these aberrations. However, the observed chromosomal lesions include lesions such as NPBs, MNs and nuclear buds, which strongly suggest that telomere damage gives a major contribution to this effect.

Overall, our data suggest that PML participates in physiologic telomere surveillance. Its function may be specifically relevant when the activity of telomerase is low, as in ALT cells, TERT-deficient cells or in normal cells. In fact, PML depletion in

telomerase-positive tumor cells does not lead to proliferation arrest or senescence (our unpublished results). PML may function by participating in the surveillance of telomeric chromatin, since the induction of an ALT phenotype was reported upon depletion of the histone chaperone ASF1.[49]

The APL-specific PML/RARα chimeric protein acts as an abnormal chromatin regulator.[50–52] Indeed this fusion protein can be considered as a dominant negative PML mutant, since it disrupts PML-NBs.[25] We found that the telomeric localization of PML is markedly impaired in normal HPCs expressing the PML/RARα protein. This finding may imply that the integrity of the protein interactions of PML and its effects on sumoylation, which are altered by the PML/RARα protein, are required for PML telomeric function. Interestingly, APL blasts have shortened telomeres,[42] suggesting that the decreased PML function may impact on telomere stability. Pre-leukemic bone marrow cells derived from mice transplanted with hematopoietic precursors expressing PML/RARα show a reduction in telomere length. Thus, before the development of a full-blown leukemia phenotype, PML/RARα expression alone induces telomere shortening. This is associated with the displacement of PML from telomeres, suggesting that the dominant negative effect of PML/RARα on PML may impair telomere surveillance, contributing to the pathogenesis of leukemia. APL typically displays a 15;17 chromosomal translocation. However, complex chromosomal abnormalities are detected in about 30% of the cases.[53,54] In the remaining patients, the impaired telomeric surveillance may not translate in complex chromosomal aberrations due to the rapid natural history of this leukemia or the effective treatment.

Overall, our data identify a novel and important functional role for PML in telomeres surveillance in normal cells and imply that a diminished PML function may contribute to cell senescence, genomic instability and tumorigenesis.

MATERIALS AND METHODS

Primary cells and cell lines

293 T packaging cells, HeLa cells, the lung carcinoma A549 and the osteosarcoma U2OS cell lines and normal human WI38 fibroblasts were maintained in Dulbecco's Modified Eagle's Medium supplemented with 10% fetal bovine serum (EuroClone, Pero, Italy). MRC-5 normal human fibroblasts and the lung adenocarcinoma cell line SK-LU-1 were cultured in Eagle's Minimum Essential Medium (EuroClone) with the above supplementation, non-essential amino acids (0.1 mM) (EuroClone) and sodium pyruvate (1 mM) (EuroClone). The osteosarcoma cell line Saos-2 was cultured in McCoy's Medium (Sigma-Aldrich, St Louis, MO, USA) supplemented with 15% fetal bovine serum. Media were supplemented with penicillin (100 units/ml) and streptomycin (100 μg/ml, EuroClone). All cells were cultured in 5% CO_2 at 37 °C. Cell lines were purchased from American Type Culture Collection (ATCC) Manassas, VA, USA). Mouse embryonic fibroblasts were isolated from in house animals, following standard procedures, from embryos surgically removed at embryonic day 13.5 and cultured in Dulbecco's Modified Eagle's Medium supplemented with antibiotics and 10% fetal bovine serum, in 9% CO_2 at 37 °C. Late passage near senescent MRC5 and WI38 cells (NS) are defined as passages 30–34, corresponding to about 35–40 population doublings, when the cells decrease their proliferation rate to about one half of early passage cells. For colony assays 0.5×10^3 HeLa cells were plated in triplicate in 6 cm plates in growth medium. Ten days after plating, colony number was evaluated. The cells were washed twice with PBS, fixed in 5% formaldehyde, rinsed and stained for 5 min with 0.05% crystal violet. Visible colonies were counted. The experiments were repeated at least three times. Mean and s.d. were calculated among the experiments.

RHPS4 and blebbistatin

The G-quadruplex ligand RHPS4[38,39] was added directly to the culture medium at the concentration of 1 μM for 24 h to induce specific telomeric DNA damage in human fibroblasts. Blebbistatin 20 μM (Sigma-Aldrich) was added to the culture medium for 24 h to block cytokinesis. All experiments were performed at least three times.

Lentiviral vectors constructs and siRNA for RNA interference

The following oligonucleotides were used to generate shRNAs for PML, TRF2 and a control luciferase sequence (Luc). (Eurofins MWG Operon, Ebersberg, Germany).

PMLKD1: For 5′-TGACCTCAGCTCTTGCATCATTCAAGAGATGATGCAAGAGCT GAGGTCTTTTTTC3′; Rev 5′-TCGAGAAAAAAGACCTCAGCTCTTGCATCATCTCTTG AATGATGCAAGAGCTGAGGTCA-3′; PMLKD2: For 5′-TGGGACCCTATTGACGTTG ATTCAAGAGATCAACGTCAATAGGGTCCCTTTTTTC-3′; Rev 5′-TCGAGAAAAAAG GGACCCTATTGACGTTGATCTCTTGAATCAACGTCAATAGGGTCCCA-3′; LUC: For 5′-TCTTACGCTGAGTACTTCGATTCAAGAGATCGAAGTACTCAGCGTAAGTTTTTTC -3′; Rev 5′-TCGAGAAAAAACTTACGCTGAGTACTTCGATCTCTTGAATCGAAGTAC TCAGCGTAAGA-3′; TRF2 KD: For 5′-TGAGGATGAACTGTTTCAAGTTCAAGAGAC TTGAAACAGTTCATCCTCTTTTTTC-3′; Rev 5′-TCGAGAAAAAAGAGGATGAACTG TTTCAAGTCTCTTGAACTTGAAACAGTTCATCCTCA-3′.

Oligonucleotides were annealed and cloned into pSIcoR vectors.[55] Lentiviral particles were generated in 293 T cells by standard methods and used for infection.[56] Infected cells were selected with puromycin for 3 days and selection was confirmed by the death of puromycin-treated uninfected cells.

Oligonucleotide sequences used for siRNA experiments were the following. Luciferase (Luc): 5′-CTTACGCTGAGTACTTCGA-3′; PMLKD1: 5′-GACCTCAGCTCTTGCATCA-3′; PML KD2: 5′-GGGACCCTATTGACGTTGA-3′. SiRNA was transfected at 20 nM using Lipofectamine RNAi MAX kit (Invitrogen, Carlsbad, CA, USA) following the manufacturer protocol.

Growth curves and β-galactoside assays

Primary fibroblasts were seeded in 6-well plates, in triplicate. Cells were counted at 3, 6, 8 and 10 days after plating for growth curves evaluation. For β-galactoside staining, the cells were washed in PBS (EuroClone), fixed with 4% paraformaldehyde and incubated overnight at 37 °C in staining buffer (1 mg/ml 5-bromo-4-chloro-3-indolyl β-D- galactoside (X-Gal), 5 mM potassium ferrocyanide, 40 mM citric acid, 150 mM $NaCl_2$, 2 mM $MgCl_2$ and sodium phosphate pH 6.0). At the end of incubation, cells were washed with PBS and analyzed.[57] All the experiments were performed at least three times.

Immunofluorescence and microscopy

Cells were grown directly on glass coverslips, fixed with 4% paraformaldehyde, permeabilized in PBS containing 0.1% Triton X-100 (Sigma-Aldrich) and blocked 1 h in blocking solution (PBS 2% BSA). The cells were then stained with a primary antibody for 1 h at room temperature and counterstained with a secondary antibody. Cell nuclei were stained with 4′,6-diamidino-2-phenylindole (DAPI). Images were captured with a CCD (charge-coupled device) camera (Hamamatsu Bs/W CCD Camera CJ895, Hamamatsu Photonics Italia, Milano, Italy), using a wide field (Olympus BX61, Olympus Italia, Segrate, Italy) or a confocal (Leica TCS SP2 AOBS, Leica Microsystem, Milano, Italy) microscope. Supplementary Figure 2 and Supplementary Video 1 show the criteria for colocalization scoring. *In situ* 53BP1-Trf2 PLA was performed as described.[36,37] Coverslips for detection of cell-cycle distribution by wide field high-resolution cytometry were stained with DAPI (10 μM for 30 min) and mounted in a Mowiol containing mounting media. DNA counterstain for confocal analysis was performed by incubating cells with Chromomycin A3 (10 μM in PBS/70 mM $MgCl_2$) or Draq5 and mounting coverslips in a DABCO containing glycerol-based mounting medium to preserve cell 3D structure. Primary antibodies used were anti-PML (H238, sc-5621, Santa Cruz Biotechnology, Dallas, TX, USA) (PGM3, sc-100410, Santa Cruz Biotechnology), anti-γH2AX (Ser139) (Upstate 05-636, Millipore, Billerica, MA, USA), anti-TRF2 (clone 4A794, Millipore) rabbit anti-53BP1 (ab36823, Abcam, Cambridge, UK) and anti-p53 (DO-1, sc-126, Santa Cruz Biotechnology). Secondary antibodies used were CY3 donkey anti-Rabbit/Mouse, CY5 donkey anti-Rabbit/Mouse (Jackson Immunoresearch, West Grove, PA, USA), Alexa488 donkey anti-Rabbit/Mouse (Alexa) and Pacific Orange anti-Rabbit/Mouse (Jackson Immunoresearch).

Image cytometry analysis

The image cytometry experiments for simultaneous detection of cell-cycle distribution, DNA replication, PML and telomeres content and spatial localization were performed as described.[36,37] Automated wide field and confocal microscopes acquired images were analyzed by an ad-hoc image analysis software developed in the ImageJ macro language. Since the frequency of the detected events was particularly low in the exponential growth phase, we increased the throughput of the confocal analysis employing wide field microscopy to measure up to 15 000 cells. To increase

efficiency in the high-resolution detection of damaged telomeres, we employed PLA between TRF2 and 53BP1 protein (see Immunofluorescence). To evaluate cell-cycle distribution, cells were classified according to the DNA and EdU content (G1: 2 N EdU negative; G2: 4 N EdU negative; S phase: EdU positive). Spots were detected by first applying a Laplace of Gaussian filter on background-subtracted images. Colocalization between targeted spots (PLA (damaged telomeres) and PML-NBs) was considered by calculating mutual distances of the fluorescence barycenter ranging between 100 (colocalization) and 400 nm (less than sum of the spots radius) (Figure 2b).

Immuno-FISH staining and telomere FISH. Cultured cells were fixed in 4% paraformaldehyde for 30′ and 100 mM glycine for 20′ at room temperature. The cells were then permeabilized in 0.5% Triton X-100/0.5% saponin. Primary and secondary antibody staining was performed as described above and followed by an additional fixation with 4% paraformaldehyde and 100 mM glycine. Telomere-FISH was carried out using the Telomere PNA FISH Kit/Cy3 (DAKO, Glostrup, Denmark), according to the manufacturer protocol. Briefly, slides were immersed in Tris-buffered Saline and permeabilized with pretreatment solution. DNA was denatured by heating 5 min at 80 °C in hybridization solution (50% formamide, 20% dextran sulfate in ×2 SSC) containing a Cy3-conjugated PNA probe specific for telomeric repeats. After the annealing step at RT in the dark, the slides were washed with Tris-buffered Saline, counterstained with DAPI and mounted in Mowiol. Images were collected as described above and ImageJ software (W. Rasband, NIH) was used to process and analyze images. Experiments performed with this technique shown in the manuscript are representative of three experiments. As described in figure legends, statistics were carried out scoring nuclei 50–100/condition in every triplicate experiment.

Binucleation assay for abnormal nuclear morphology analysis

MRC-5 cells were grown on cover slips and transfected with 20 nM siRNA targeting PML. Twelve hours later, cells were treated with 20 μM Blebbistatin (Sigma-Aldrich) for 24 h to block cytokinesis, fixed in 4% paraformaldehyde and stained for Immunofluorescence as described above. The analysis of abnormal nuclear morphologies was performed on binucleated cells using described criteria.[58] An NPB was considered to be the narrow/wide chromatin segment connecting two cell nuclei, MNs were morphologically identical to, but smaller than the cell nucleus, and round and oval protrusions of the nuclear membrane, connected to the cell nucleus, were classified as buds.[59] The experiments were performed at least three times. In every experiment 50 binucleated cells were analyzed.

Metaphase spreads

Metaphase spreads were obtained from MRC-5 PML knockdown cells treated with 0.1 μg/ml colcemid (Gibco, Carlsbad, CA, USA) for 2 h. Cells were trypsinized, washed in PBS and incubated in hypotonic solution (75 mM KCl) for 30 min at 37 °C. The cells were then fixed with methanol/glacial acetic acid (3:1 vol/vol). For telomeric FISH, the cells were either spun onto coverslips via a cytospin centrifuge or spread across a slide presoaked in 2% TWEEN detergent (Sigma-Aldrich) and dried. Staining was performed with a specific telomeric PNA probe as above. Fifty metaphases were analyzed in each of three experiments.

Western blotting

Western blotting was performed as described previously.[60] The primary antibodies used were anti-PML (H238, sc-5621, Santa Cruz Biotechnology), anti-TRF2 (clone 4A794, Millipore), anti-p53 (DO-1, sc-126, Santa Cruz Biotechnology), anti-p21 (C-19, sc-397, Santa Cruz Biotechnology), anti-p16 (H-156, sc-759, Santa Cruz Biotechnology), anti-vinculin or anti-actin (Santa Cruz Biotechnology) were used to normalize protein content of samples. Images shown in the figures are representative of at least three experiments.

Isolation of primary T-lymphocytes

Peripheral blood mononuclear cells were obtained after informed consent from a patient carrying a germline X456Y mutation in the TERT gene and from an age-matched control donor. The cells were isolated by centrifugation on Ficoll–Hypaque (Pharmacia, Uppsala, Sweden) and cultured in RPMI-1640 supplemented with 10% FCS and penicillin/streptomycin antibiotics (EuroClone). Monocytes were depleted by plastic adherence and T-lymphocytes were activated for 16 h by 5 mg/ml phytohaemoagglutinin A (Pharmacia) and then stimulated with interleukin-2 (500 U/ml) (Pharmacia). Immuno-FISH experiments were performed on cytospin slides.

Statistical significance

Where indicated data represented as mean ± s.d. were derived from at least three independent experiments. Statistical significance between means was assessed by Student's *t*-test where a *P*-value of < 0.05 was considered as significant.

Human CD34+ hematopoietic progenitors purification and retroviral infection

CD34+ cells were purified, cultured *in vitro* and transduced with a control or a PML/RARα cDNA containing retroviral vector, as previously described,[61] but using a pBABE-Puro retrovirus vector backbone. Twenty-four hours after the infection, the cells were selected in puromycin for 48 h. Immuno-FISH experiments on CD34+ cells were performed as described above.

Mice transplantation and bone marrow analysis

The procedures for bone marrow isolation, transduction and transplantation were performed as described,[43] using 129/Sv inbred mice (The Jackson Laboratory, Bar Harbor, MA, USA).

Telomere length measurement assays

The average length of telomere repeats was evaluated by flow FISH[62] using a telomere-specific FITC labeled probe according to the manufacturer instructions (DAKO). Samples were then analyzed by flow cytometry (FACScan, BD Biosciences, Milano, Italy) and relative telomere length was determined by comparing isolated test cells with a control cell line (1301; sub-line of the Epstain-Barr Virus genome negative T-cell leukemia line CCRF-CEM).

CONFLICT OF INTEREST

The authors declare no conflict of interest.

ACKNOWLEDGEMENTS

This work was supported by AIRC IG grant to FG, and SM, and by a grant from the Fondazione Cassa di Risparmio di Perugia to FG. We thank Lucilla Luzi and Alessandro Brozzi (European Institute of Oncology, Milan) for their help in statistical analysis and Annamaria Biroccio (Istituto Nazionale Tumori Regina Elena, Roma) for kindly providing us the RHPS4 compound. We are grateful to Simona Colla (MD Anderson Cancer Center) for encouragement and critical reading of the manuscript, to Giulio Draetta and Luigi Nezi (MD Anderson Cancer Center) for their encouragement and support. This work was supported by AIRC IG grant to FG, and SM, and by a grant from the Fondazione Cassa di Risparmio di Perugia to FG.

REFERENCES

1 Akbar AN, Vukmanovic-Stejic M. Telomerase in T lymphocytes: use it and lose it? *J Immunol* 2007; **178**: 6689–6694.
2 Bailey SM, Meyne J, Chen DJ, Kurimasa A, Li GC, Lehnert BE *et al.* DNA double-strand break repair proteins are required to cap the ends of mammalian chromosomes. *Proc Nati Acad Sci USA* 1999; **96**: 14899–14904.
3 Nandakumar J, Cech TR. Finding the end: recruitment of telomerase to telomeres. *Nat Rev Mol Cell Biol* 2013; **14**: 69–82.
4 d'Adda di Fagagna F, Reaper PM, Clay-Farrace L, Fiegler H, Carr P, Von Zglinicki T *et al.* A DNA damage checkpoint response in telomere-initiated senescence. *Nature* 2003; **426**: 194–198.
5 Takai H, Smogorzewska A, de Lange T. DNA damage foci at dysfunctional telomeres. *Curr Biol* 2003; **13**: 1549–1556.
6 Stagno D'Alcontres M, Mendez-Bermudez A, Foxon JL, Royle NJ, Salomoni P. Lack of TRF2 in ALT cells causes PML-dependent p53 activation and loss of telomeric DNA. *J Cell Biol* 2007; **179**: 855–867.
7 Karlseder J, Smogorzewska A. de Lange T. Senescence induced by altered telomere state, not telomere loss. *Science* 2002; **295**: 2446–2449.
8 Hayflick L, Moorhead PS. The serial cultivation of human diploid cell strains. *Exp Cell Res* 1961; **25**: 585–621.
9 Harley CB, Futcher AB, Greider CW. Telomeres shorten during ageing of human fibroblasts. *Nature* 1990; **345**: 458–460.
10 Allsopp RC, Vaziri H, Patterson C, Goldstein S, Younglai EV, Futcher AB *et al.* Telomere length predicts replicative capacity of human fibroblasts. *Proc Nati Acad Sci USA* 1992; **89**: 10114–10118.
11 Kuilman T, Michaloglou C, Mooi WJ, Peeper DS. The essence of senescence. *Genes Dev* 2010; **24**: 2463–2479.
12 Armanios M. Telomeres and age-related disease: how telomere biology informs clinical paradigms. *J Clin Invest* 2013; **123**: 996–1002.

13 Newgard CB, Sharpless NE. Coming of age: molecular drivers of aging and therapeutic opportunities. *J Clin Invest* 2013; **123**: 946–950.
14 van Deursen JM. The role of senescent cells in ageing. *Nature* 2014; **509**: 439–446.
15 Greider CW, Blackburn EH. Identification of a specific telomere terminal transferase activity in Tetrahymena extracts. *Cell* 1985; **43**: 405–413.
16 Flores I, Benetti R, Blasco MA. Telomerase regulation and stem cell behaviour. *Curr Opin Cell Biol* 2006; **18**: 254–260.
17 Kim NW, Piatyszek MA, Prowse KR, Harley CB, West MD, Ho PL *et al.* Specific association of human telomerase activity with immortal cells and cancer. *Science* 1994; **266**: 2011–2015.
18 Bryan TM, Englezou A, Dalla-Pozza L, Dunham MA, Reddel RR. Evidence for an alternative mechanism for maintaining telomere length in human tumors and tumor-derived cell lines. *Nat Med* 1997; **3**: 1271–1274.
19 Cesare AJ, Reddel RR. Alternative lengthening of telomeres: models, mechanisms and implications. *Nat Rev Genet* 2010; **11**: 319–330.
20 Yeager TR, Neumann AA, Englezou A, Huschtscha LI, Noble JR, Reddel RR. Telomerase-negative immortalized human cells contain a novel type of promyelocytic leukemia (PML) body. *Cancer Res* 1999; **59**: 4175–4179.
21 Pandolfi PP, Grignani F, Alcalay M, Mencarelli A, Biondi A, LoCoco F *et al.* Structure and origin of the acute promyelocytic leukemia myl/RAR alpha cDNA and characterization of its retinoid-binding and transactivation properties. *Oncogene* 1991; **6**: 1285–1292.
22 de The H, Lavau C, Marchio A, Chomienne C, Degos L, Dejean A. The PML-RAR alpha fusion mRNA generated by the t(15;17) translocation in acute promyelocytic leukemia encodes a functionally altered RAR. *Cell* 1991; **66**: 675–684.
23 Kakizuka A, Miller Jr WH, Umesono K, Warrell Jr RP, Frankel SR, Murty VV *et al.* Chromosomal translocation t(15;17) in human acute promyelocytic leukemia fuses RAR alpha with a novel putative transcription factor, PML. *Cell* 1991; **66**: 663–674.
24 Goddard AD, Borrow J, Freemont PS, Solomon E. Characterization of a zinc finger gene disrupted by the t(15;17) in acute promyelocytic leukemia. *Science* 1991; **254**: 1371–1374.
25 de The H, Le Bras M, Lallemand-Breitenbach V. The cell biology of disease: Acute promyelocytic leukemia, arsenic, and PML bodies. *J Cell Biol* 2012; **198**: 11–21.
26 Pearson M, Pelicci PG. PML interaction with p53 and its role in apoptosis and replicative senescence. *Oncogene* 2001; **20**: 7250–7256.
27 Carbone R, Pearson M, Minucci S, Pelicci PG. PML NBs associate with the hMre11 complex and p53 at sites of irradiation induced DNA damage. *Oncogene* 2002; **21**: 1633–1640.
28 Dellaire G, Ching RW, Ahmed K, Jalali F, Tse KC, Bristow RG *et al.* Promyelocytic leukemia nuclear bodies behave as DNA damage sensors whose response to DNA double-strand breaks is regulated by NBS1 and the kinases ATM, Chk2, and ATR. *J Cell Biol* 2006; **175**: 55–66.
29 Salomoni P, Pandolfi PP. The role of PML in tumor suppression. *Cell* 2002; **108**: 165–170.
30 Mazza M, Pelicci PG. Is PML a tumor suppressor? *Front Oncol* 2013; **3**: 174.
31 Slatter TL, Tan X, Yuen YC, Gunningham S, Ma SS, Daly E *et al.* The alternative lengthening of telomeres pathway may operate in non-neoplastic human cells. *J Phatol* 2012; **226**: 509–518.
32 Chang FT, McGhie JD, Chan FL, Tang MC, Anderson MA, Mann JR *et al.* PML bodies provide an important platform for the maintenance of telomeric chromatin integrity in embryonic stem cells. *Nucleic Acids Res* 2013; **41**: 4447–4458.
33 de The H, Chomienne C, Lanotte M, Degos L, Dejean A. The t(15;17) translocation of acute promyelocytic leukaemia fuses the retinoic acid receptor alpha gene to a novel transcribed locus. *Nature* 1990; **347**: 558–561.
34 Melnick A, Licht JD. Deconstructing a disease: RARalpha, its fusion partners, and their roles in the pathogenesis of acute promyelocytic leukemia. *Blood* 1999; **93**: 3167–3215.
35 Gunes C, Rudolph KL. The role of telomeres in stem cells and cancer. *Cell* 2013; **152**: 390–393.
36 Furia L, Pelicci PG, Faretta M. A computational platform for robotized fluorescence microscopy (I): high-content image-based cell-cycle analysis. *Cytometry A* 2013; **83**: 333–343.
37 Furia L, Pelicci PG, Faretta M. A computational platform for robotized fluorescence microscopy (II): DNA damage, replication, checkpoint activation, and cell cycle progression by high-content high-resolution multiparameter image-cytometry. *Cytometry A* 2013; **83**: 344–355.
38 Leonetti C, Amodei S, D'Angelo C, Rizzo A, Benassi B, Antonelli A *et al.* Biological activity of the G-quadruplex ligand RHPS4 (3,11-difluoro-6,8,13-trimethyl-8H-quino[4,3,2-kl]acridinium methosulfate) is associated with telomere capping alteration. *Mol Pharmacol* 2004; **66**: 1138–1146.
39 Salvati E, Leonetti C, Rizzo A, Scarsella M, Mottolese M, Galati R *et al.* Telomere damage induced by the G-quadruplex ligand RHPS4 has an antitumor effect. *J Clin Invest* 2007; **117**: 3236–3247.
40 van Steensel B, Smogorzewska A, de Lange T. TRF2 protects human telomeres from end-to-end fusions. *Cell* 1998; **92**: 401–413.
41 Fenech M, Crott JW. Micronuclei nucleoplasmic bridges and nuclear buds induced in folic acid deficient human lymphocytes-evidence for breakage-fusion-bridge cycles in the cytokinesis-block micronucleus assay. *Mutat Res* 2002; **504**: 131–136.
42 Ghaffari SH, Shayan-Asl N, Jamialahmadi AH, Alimoghaddam K, Ghavamzadeh A. Telomerase activity and telomere length in patients with acute promyelocytic leukemia: indicative of proliferative activity, disease progression, and overall survival. *Ann Oncol* 2008; **19**: 1927–1934.
43 Minucci S, Monestiroli S, Giavara S, Ronzoni S, Marchesi F, Insinga A *et al.* PML-RAR induces promyelocytic leukemias with high efficiency following retroviral gene transfer into purified murine hematopoietic progenitors. *Blood* 2002; **100**: 2989–2995.
44 Slatter T, Gifford-Garner J, Wiles A, Tan X, Chen YJ, MacFarlane M *et al.* Pilocytic astrocytomas have telomere-associated promyelocytic leukemia bodies without alternatively lengthened telomeres. *Am J Pathol* 2010; **177**: 2694–2700.
45 Verdun RE, Crabbe L, Haggblom C, Karlseder J. Functional human telomeres are recognized as DNA damage in G2 of the cell cycle. *Mol Cell* 2005; **20**: 551–561.
46 Berardinelli F, Antoccia A, Cherubini R, De Nadal V, Gerardi S, Cirrone GA *et al.* Transient activation of the ALT pathway in human primary fibroblasts exposed to high-LET radiation. *Radiat Res* 2010; **174**: 539–549.
47 Armanios M, Blackburn EH. The telomere syndromes. *Nat Rev Genet* 2012; **13**: 693–704.
48 Dellaire G, Bazett-Jones DP. PML nuclear bodies: dynamic sensors of DNA damage and cellular stress. *Bioessays* 2004; **9**: 963–977.
49 O'Sullivan RJ, Arnoult N, Lackner DH, Oganesian L, Haggblom C, Corpet A *et al.* Rapid induction of alternative lengthening of telomeres by depletion of the histone chaperone ASF1. *Nat Struct Mol Biol* 2014; **21**: 167–174.
50 Grignani F, De Matteis S, Nervi C, Tomassoni L, Gelmetti V, Cioce M *et al.* Fusion proteins of the retinoic acid receptor-alpha recruit histone deacetylase in promyelocytic leukaemia. *Nature* 1998; **391**: 815–818.
51 Lin RJ, Nagy L, Inoue S, Shao W, Miller Jr WH, Evans RM. Role of the histone deacetylase complex in acute promyelocytic leukaemia. *Nature* 1998; **391**: 811–814.
52 He LZ, Guidez F, Tribioli C, Peruzzi D, Ruthardt M, Zelent A *et al.* Distinct interactions of PML-RARalpha and PLZF-RARalpha with co-repressors determine differential responses to RA in APL. *Nat Genet* 1998; **18**: 126–135.
53 Hiorns LR, Swansbury GJ, Mehta J, Min T, Dainton MG, Treleaven J *et al.* Additional chromosome abnormalities confer worse prognosis in acute promyelocytic leukaemia. *Br J Haematol* 1997; **96**: 314–321.
54 Pantic M, Novak A, Marisavljevic D, Djordjevic V, Elezovic I, Vidovic A *et al.* Additional chromosome aberrations in acute promyelocytic leukemia: characteristics and prognostic influence. *Med Oncol* 2000; **17**: 307–313.
55 Ventura A, Meissner A, Dillon CP, McManus M, Sharp PA, Van Parijs L *et al.* Cre-lox-regulated conditional RNA interference from transgenes. *Proc Natl Acad Sci USA* 2004; **101**: 10380–10385.
56 Vian L, Di Carlo M, Pelosi E, Fazi F, Santoro S, Cerio AM *et al.* Transcriptional fine-tuning of microRNA-223 levels directs lineage choice of human hematopoietic progenitors. *Cell Death Differ* 2014; **21**: 290–301.
57 Dimri GP, Lee X, Basile G, Acosta M, Scott G, Roskelley C *et al.* A biomarker that identifies senescent human cells in culture and in aging skin in vivo. *Proc Nati Acad Sci USA* 1995; **92**: 9363–9367.
58 Fenech M. The in vitro micronucleus technique. *Mutat Res* 2000; **455**: 81–95.
59 Gisselsson D, Bjork J, Hoglund M, Mertens F, Dal Cin P, Akerman M *et al.* Abnormal nuclear shape in solid tumors reflects mitotic instability. *Am J Pathol* 2001; **158**: 199–206.
60 Racanicchi S, Maccherani C, Liberatore C, Billi M, Gelmetti V, Panigada M *et al.* Targeting fusion protein/corepressor contact restores differentiation response in leukemia cells. *EMBO J* 2005; **24**: 1232–1242.
61 Grignani F, Valtieri M, Gabbianelli M, Gelmetti V, Botta R, Luchetti L *et al.* PML/RAR alpha fusion protein expression in normal human hematopoietic progenitors dictates myeloid commitment and the promyelocytic phenotype. *Blood* 2000; **96**: 1531–1537.
62 Rufer N, Dragowska W, Thornbury G, Roosnek E, Lansdorp PM. Telomere length dynamics in human lymphocyte subpopulations measured by flow cytometry. *Nat Biotechnol* 1998; **16**: 743–747.

Supplementary Information accompanies this paper on the Oncogene website (http://www.nature.com/onc)